Stochastic Fractal Models for Image Processing

Béatrice Pesquet-Popescu[1] and Jacques Lévy Véhel[2]

[1] ENST, Signal and Image Processing Dept., 46, rue Barrault, 75634 Paris Cedex 13, France

[2] INRIA, Projet Fractales, Domaine de Voluceau, 78153 Le Chesnay Cedex, France

I. Are fractals everywhere ?

A very often cited example of a fractal curve is the Brittany coast in France. The view one has by looking at this highly irregular coast at coarse scale is indeed quite similar to what can be observed by looking more precisely at a small part of the sea shore. In a famous book [1], it was further claimed that *fractals are everywhere*.

Actually, in the last years, image processing using fractal models has represented an active research area stimulated by the plethora of applications [2] (infographics [3], geophysics [4], [5], turbulence phenomena [6], [7], satellite imagery, texture modeling, classification and segmentation [8], [9], compression, watermarking, ...) where these concepts are potentially interesting. Fractals correspond to the general idea – that can be easily understood from an intuitive point of view – that a given object, especially a textured area, can be represented by similar characteristics "repeated" at different scales. This versatile idea can however be translated into different forms from a mathematical point of view. In this tutorial, we will be mainly interested in a stochastic view of fractals, which will focus on more or less sophisticated models for describing image textures. As will be shown in this paper, these models rely on the notion of statistical "self-similarity". This concept is at the origin of relevant models for several natural phenomena. In the meantime, the non-stationary structure of self-similar processes put them at the core of the most recent preoccupations in image and signal processing.

Our trip in fractal landscapes will depart from the simplest but yet effective model of fractional Brownian motion, and explore its two-dimensional extensions. We will focus on the ability to introduce anisotropy in this model and we will also be interested in considering its discrete-space counterparts. We will then move towards recent multifractional and multifractal models providing more degrees of freedom for fitting complex 2D fields.

We note in this introduction that many of the models and processing described below are implemented in FracLab, a software Matlab/Scilab toolbox for fractal processing of signals and images. FracLab is available at the following address: `http://www-rocq.inria.fr/fractales/`.

II. A simple example of a fractal field: the fractional Brownian motion

A. Reminders about the 1D fBm

Fractional Brownian motion (fBm) is one of the most popular stochastic fractal model for images. It was introduced by Kolmogorov and studied by Mandelbrot and Van Ness in 1968 [4]. It is a nonstationary process, but it has stationary increments. In 1D, it is the only self-similar (i.e. "fractal") Gaussian process with stationary increments.

Let us briefly remind some of the most important properties of the one-dimensional fBm, in order to compare and to extend it to two (or higher) dimensions. A process $\{B_H(t), t \in \mathbb{R}\}$ is a 1D fBm if it is Gaussian, zero-mean and its autocorrelation function is given by

$$R_{B_H}(t,s) = \mathrm{E}\{B_H(t)B_H(s)\} = \frac{\sigma^2}{2}\left[|t|^{2H} + |s|^{2H} - |t-s|^{2H}\right], \quad (1)$$

where $0 < H < 1$ is the fractal scaling parameter, also called the Hurst parameter. For $H = 1/2$ we obtain the well known Brownian motion (or Wiener process), denoted by $B(t)$. One of the most important properties of the Brownian motion is the independence of its increments.

The fBm is a random process which is continuous in the mean-square sense. It admits several integral representations. The most popular one, as introduced in [4], is:

$$B_H(t) \propto \int_{-\infty}^{0} \left[(t-s)^{H-1/2} - (-s)^{H-1/2}\right] dB(s) + \int_0^t (t-s)^{H-1/2} dB(s). \quad (2)$$

(2) allows to interpret the fBm as a *derivative of fractional order* $1/2 - H$ of Brownian motion. Another useful representation is the "spectral representation" of the fBm [10].

The so-called "power law" or "T^H law" of the fBm states that the variance of the increments of $B_H(t)$ is given by $\mathrm{E}\{[B_H(t+\tau) - B_H(t)]^2\} = \sigma^2|\tau|^{2H}$. We will call this quantity the "structure function" of the fBm. As will be seen in Section III-A, it also plays an important role in the study of more general processes with stationary increments. As the fBm is nonstationary (and therefore one cannot define its power spectrum), but it has stationary increments, it is more convenient to study the characteristics of this process using the autocorrelation and the spectrum of its increments. This approach was used in [11] to define the "generalized power spectrum" of $B_H(t)$, which is proportional to $|\omega|^{-(2H+1)}$, $0 < H < 1$.

The first order increment of the sampled fBm is the *fractional Gaussian noise (fGn)*: $G_H(k) = \Delta B_H(k;1) = B_H(k) - B_H(k-1)$, $k \in \mathbb{Z}$. It is a stationary process, whose autocorrelation function decays hyperbolically as $|k|^{2H-2}$ (for $H \neq 1/2$), and therefore the discrete-time process exhibits a short-range dependence for $0 < H < 1/2$, independence for $H = 1/2$ (Brownian motion) and long-range dependence for $1/2 < H < 1$ (see Section VI-A for more

details). Moreover, as all second order self-similar processes with stationary increments have the same second-order statistics as the fBm, it follows that their increments have all the same autocorrelation function as the fGn. The power spectrum density (psd) of the fGn is given by: $\mathcal{S}(\omega) \propto \frac{1}{|\omega|^{2H-1}}$.

Another important property of fBm is that its local regularity, as measured by the Hölder exponent α [12], is with probability one equal to H everywhere. Let us explain the geometrical meaning of this statement. Roughly speaking, saying that a function f has exponent α at t_0 means that, around t_0, the graph of f "looks like" the curve $t \mapsto f(t_0) + c|t - t_0|^\alpha$ in the following sense: For any positive ε, there exists a neighbourhood of t_0 such that the path of f inside this neighbourhood is included in the envelope defined by the two curves $t \mapsto f(t_0) + c|t - t_0|^{\alpha-\varepsilon}$ and $t \mapsto f(t_0) - c|t - t_0|^{\alpha-\varepsilon}$, while this property is no longer true for any negative ε (see figure 1). Thus, a "large" α means that f is smooth at t_0, while an irregular behaviour of f at t_0 translates into α close to 0. For instance, in 2D, pixels having an exponent smaller than 2 are "irregular", while an image is smooth in regions where all the pixels have $\alpha > 2$. In the case of fBm, $\alpha(t_0) = H$ for all t_0 with probability 1, and thus the larger H is, the smoother the path of the process will look.

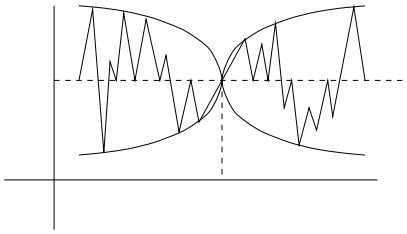

Fig. 1. Graphical interpretation of the Hölder regularity of a function f at a point t_0.

The classical one-dimensional fBm can be generalized to images or multidimensional processes in several ways, depending on the property one is looking for.

B. Multi-dimensional extensions of the fBm

Let us first keep in mind the Gaussianity assumption in the original definition of the 1D fBm and describe the corresponding processes by their correlation function. The extension to two or higher dimensions is however not unique. For example, a possible generalization is the *multi-parameter* Wiener process, or Brownian sheet, denoted by $\{W_{\mathbf{H}}(\boldsymbol{x}), \boldsymbol{x} \in \mathbb{R}^N\}$. It is an anisotropic extension, that may have different Hurst parameters in each of the N directions, gathered in the vector parameter $\mathbf{H} = (H_1, \ldots, H_N)$. The idea to generalize the definition of fBm in Eq. (1) is here to set the covariance between the points $\mathbf{x} = (x_i)_{1 \le i \le N}$ and $\mathbf{y} = (y_i)_{1 \le i \le N}$ in $\mathbb{R}^N$ equal to the product of covariances between the components of the two vectors. This is similar to what is done for defining the Brownian sheet. We get the *fractional Brownian sheet*, which is thus defined to be the centered Gaussian process with covariance function

$$E\left\{F_{\mathbf{H}}(\mathbf{x}) F_{\mathbf{H}}(\mathbf{y})\right\} \propto \prod_{i=1}^{N} \left(|x_i|^{2H_i} + |y_i|^{2H_i} - |x_i - y_i|^{2H_i}\right).$$

This field also admits a harmonizable representation, which is a separable extension of the 1D one.

Another generalization of an fBm for 2D surfaces, called *isotropic fractional Brownian field* or *Lévy fractional Brownian field*, is the Gaussian zero-mean field B_H with autocorrelation function

$$R_{B_H}(\mathbf{x}, \mathbf{y}) \propto \left(\|\mathbf{x}\|^{2H} + \|\mathbf{y}\|^{2H} - \|\mathbf{x} - \mathbf{y}\|^{2H}\right), \qquad (3)$$

where $0 < H < 1$ and $\|\cdot\|$ is the usual Euclidean norm in $\mathbb{R}^2$. Note that the one-dimensional process obtained by "cutting" an isotropic 2D fBm with a line passing through the origin of the plane is a 1D fBm with the same self-similarity index. As said above, the interpretation of the parameter H is related to the "roughness" of the fBm image: the closer H to 0, the rougher the image (the more similar to a white noise) and the closer H to 1, the smoother the corresponding texture (cf Fig. 2).

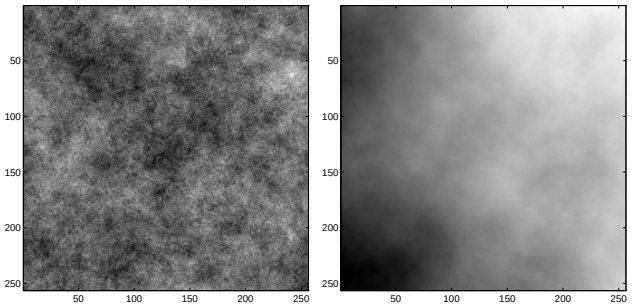

Fig. 2. Isotropic fBm's with Hurst parameters respectively $H = 0.2$ and 0.8.

The two (or n)-dimensional isotropic fBm can also be defined, as in the 1D case, as a stochastic integral existing in the mean-square sense [11]. The basic interpretation of such a construction is that the increments of the fBm are generated by passing a 2D white noise through a bidimensional fractional filter. For an isotropic field, the fractional filter is defined by its frequency response: $G(\boldsymbol{\omega}) = \|\boldsymbol{\omega}\|^{1-H-N/2}$ where N is the dimension of the space ($N = 2$ for images). Using this construction, *Reed et al.* [11] defined a generalized power spectrum of an n-dimensional fBm as $\Phi_{B_H}(\boldsymbol{\omega}) = \|\boldsymbol{\omega}\|^{-2H-N}$.

Alternatively, one can give an interpretation of the Fourier transform of the correlation function (3) in terms of a "power spectrum density" defined as the Fourier transform of a tempered distribution. Using this result, one can establish a link between the so-obtained "power spectrum" of the fBm and the expression of the averaged Wigner-Ville spectrum of the fBm introduced by Flandrin [13]. One shows [14] that the expected value of the Wigner-Ville distribution [15] of the 2D fBm is the inverse Fourier transform of this "power spectrum". Moreover, the averaged Wigner-Ville spectrum being defined as a spatial mean of the average of the Wigner-Ville distribution, it follows that the

averaged power spectrum of the 2D fBm is, for all non-zero frequencies, proportional to $\|\boldsymbol{\omega}\|^{-2H-2}$, which is also formally consistent with the previous expression of $\Phi_{B_H}(\boldsymbol{\omega})$.

Another possibility for building multidimensional extensions of the 1D fBm is to define self-similar fields with stationary 2D increments. The definition of the self-similarity in the multidimensional case is analogous to the one in 1D: *Let $F(\boldsymbol{x})$, $\boldsymbol{x} \in \mathbb{R}^2$, be a continuous-space random field. It is called self-similar of parameter $H > 0$ if, for all $a > 0$ we have $F(a\boldsymbol{x}) \stackrel{d}{=} a^H F(\boldsymbol{x})$, where $\stackrel{d}{=}$ means the equality of all its finite-dimensional probability distributions.* This implies that the statistical characteristics of the process are invariant (up to a multiplicative constant) under scale changes. The extension of the notion of stationary increments is a little bit more tricky and, depending on the definition, one can be led to fields with different properties. For example, in 1D, one can see the (strict sense) stationarity of the increments as the invariance of their probability distribution to translations (which are the only rigid body motions in a space with only one dimension). In two dimensions, the extension of this property can be seen as the invariance of the probability distribution of the increments $F(\boldsymbol{x})-F(\boldsymbol{0})$ with respect to all possible rigid body motions (translations, rotations and compositions of these operations). In the sense of this definition, the isotropic fractional Brownian motion is the only self-similar *Gaussian* field with stationary increments. If we relax the Gaussianity constraint, there exist several self-similar fields with (strict-sense) stationary increments [10], [16]. In particular, they may have stable distributions. Even though the stable fields discussed in [10] have not been used in many image processing applications, the extension of Gaussian models to heavy-tailed distributions for images is a very promising research problem which has received recently an increasing interest. Some hints on the on-going developments will be given in Section VI-D.

Besides, if the stationarity is defined not w.r.t. all the rigid body motion, but only w.r.t. translations, we come up with another definition, discussed in Section III-A.

III. Looking at Anisotropy

The extension from isotropic to anisotropic fractal image models can be realized in several ways. A first method is to build anisotropic fields by linear spatial transforms of isotropic fractal fields. This approach is discussed in Section III-B. Another possible construction is by spatial filtering of fields with desired characteristics (see Section III-B). Last, but not least, it is possible to adopt a direct approach by building intrinsically anisotropic fields, as it was done for building the fractional Brownian sheet. Another example of a direct construction will be discussed in Section III-A. In all these constructions, the structure function of the fields will play an important role in introducing and characterizing the anisotropy.

A. Fields with stationary increments of fractional order

As mentioned above, the manner of defining increments in $\mathbb{R}^2$ is important, as it leads to fields with different properties. By taking different orders of differencing along two orthogonal directions of space, we are emphasizing the anisotropy of the fields under study. This enables the construction of self-similar Gaussian fields with stationary increments other than the isotropic fBm [17].

Consider an arbitrary spatial direction (Δ_x, Δ_y). Basically, the increments $\Delta^{(D,D')}F(x,y;\Delta_x,\Delta_y)$ of fractional order $(D,D') \in \mathbb{R}_+^2$ of a 2D continuous (resp. discrete) random field $F(x,y)$ are obtained by filtering $F(x,y)$ with a linear filter whose transfer function is $\left(1-e^{-p\,\Delta_x}\right)^D \left(1-e^{-s\,\Delta_y}\right)^{D'}$, $\forall (p,s) \in \mathbb{C}^2$. In this framework, a zero-mean field $F(x,y)$ has (wide-sense) stationary increments of order (D,D') if it is with finite variances and, for all $(\Delta_x,\Delta_y,\Delta'_x,\Delta'_y)$, the cross-correlation of $\Delta^{(D,D')}F(x,y;\Delta_x,\Delta_y)$ and $\Delta^{(D,D')}F(x',y';\Delta'_x,\Delta'_y)$ is a function depending only on $x-x'$, $y-y'$ and $\Delta_x,\Delta_y,\Delta'_x,\Delta'_y$. More properties of such fields are discussed in [17] and [18]. In particular, the isotropic 2D fBm with parameter $0 < H < 1$ has stationary fractional increments of order $(D,0)/(0,D)$ for all $D \in \mathbb{R},\ D > H$.

A process $F(x,y)$ with stationary increments of order (1,0)/(0,1) is characterized by its structure function $\varphi(\Delta_x,\Delta_y)$, representing the variance of $F(x,y) - F(x-\Delta_x, y-\Delta_y)$ for all (Δ_x,Δ_y). This function is also used in geostatistics problems [19], and for characterizing the roughness of mechanical surfaces, which are by their nature anisotropic and non-stationary [20]. The structure function is a fundamental concept, as it can be used to express the autocorrelation function of the fields with stationary increments, which shows that zero-mean Gaussian fields with stationary increments are entirely characterized by this function. Moreover, one can determine explicitly the form of the structure function of such a field having self-similar properties. More precisely, its expression reads: $\varphi(x,y) = \rho^{2H} f(\theta)$, where $0 < H < 1$, $\rho = \sqrt{x^2+y^2}$, $\theta = \text{angle}(x+jy)$ and f is a π-periodic function. For example, the function f reduces to a constant in the case of isotropic fBm.

B. Filtering and Linear Spatial Transforms

If we consider a second order random field $F(\mathbf{x})$, $\mathbf{x} \in \mathbb{R}^2$, with stationary increments of order (1,0)/(0,1) and such that $F(\mathbf{0}) = \mathbf{0}$, we can build the field $G(\mathbf{x}) = \int_{\mathbb{R}^2} h(\mathbf{u}) F(\mathbf{x}-\mathbf{u}) d\mathbf{u}$, where h is the impulse response of the considered real filter. Provided that h decays fast enough, the existence of this field is guaranteed [14]. It has also stationary increments of order (1,0)/(0,1) and its structure function can be easily deduced from the structure function of the field F.

Another way of introducing the anisotropy is to observe that, if $\varphi_F(\boldsymbol{\Delta})$, $\boldsymbol{\Delta} \in \mathbb{R}^2$, is the structure function of a field $F(x,y)$ with stationary increments of order (1,0)/(0,1), then, for all 2×2 real matrix $\boldsymbol{M}$, $F(\boldsymbol{M}\mathbf{x})$ is a field with stationary increments of order (1,0)/(0,1) with structure function $\varphi_F(\boldsymbol{M}\boldsymbol{\Delta})$. Moreover, by using polar coordinates $\boldsymbol{\Delta} = \rho(\cos\theta, \sin\theta)$, the structure function of an isotropic 2D fBm takes the form : $\varphi_{B_H}(\rho) \propto \rho^{2H}$, whereas the structure function of any self-similar field with stationary incre-

ments of order $(1,0)/(0,1)$ resulting from a linear spatial transformation of the 2D fBm will be:

$$\varphi\left(\boldsymbol{M}\boldsymbol{\Delta}\right) \propto \rho^{2H}\left(1-\alpha\cos\left[2(\theta-\theta_0)\right]\right)^H. \qquad (4)$$

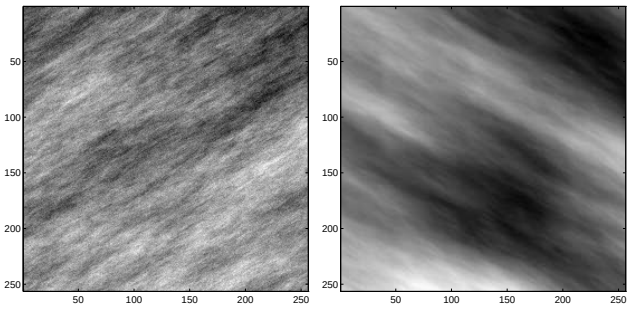

Fig. 3. Anisotropic fields with structure function given by Eq. (4), having resp. the parameters $H=0.2$, $\alpha=0.9$, $\theta_0=2\pi/3$ (left), and $H=0.8$, $\alpha=0.9$, $\theta_0=\pi/3$ (right).

The parameter $\alpha\in[0,1]$ controls the degree of anisotropy, while $\theta_0\in[0,\pi]$ indicates the "privileged" direction of the field. More precisely, the increments have the smallest (resp. largest) variation in the direction θ_0 (resp., $\theta_0+\pi/2$). The two extreme cases, $\alpha=0$ and $\alpha=1$, correspond, respectively, to an isotropic fBm and to a completely oriented field obtained by stacking 1D fBm's along each line of direction $\theta_0+\pi/2$.

IV. Is stationarity a realistic assumption?

The stationary-increments property of fBm is useful because it allows to simplify the analysis. However, most real world images do not share this property. In order to obtain realistic models, one must consider more complex processes, which have non stationary increments of any order. One of the simplest fractal models that falls into this category is the *multifractional Brownian motion* (mBm). The major difference between the two processes is that, unlike fBm, the Hölder exponent of mBm is allowed to vary along the trajectory, a useful feature when one needs to model processes whose regularity varies in space, as is the case for most images. While all the properties of fBm are governed by the unique *number* H, a *function* $H(x,y)$ is available in the case of mBm. Let us give two examples that explain why this is important. As we have seen, the long term correlations of the increments of fBm decay as $k^{(2H-2)}$, where k is the lag, resulting in long range dependence (LRD) when $H>1/2$ and anti-persistent behavior when $H<1/2$. In this respect, fBm is "degenerated": Since H rules both ends of the Fourier spectrum, i.e. the high frequencies related to the Hölder regularity and the low frequencies related to the long term dependence structure, it is not possible to have at the same time a very irregular local behavior (H close to 0) and LRD ($H>1/2$). fBm is thus not adapted to model processes which display both those features, such as Internet traffic or certain highly textured images with strong global organization, as are e.g. MR brain images. In contrast, mBm is perfectly fitted in this case. Another example is image synthesis: fBm has frequently been used for generating artificial mountains [3]. Such a modeling assumes that the irregularity of the mountain is everywhere the same. This is not realistic, since it does not take into account, e.g., erosion, which smoothes some parts of the mountains more than others. To model these and other fine features of landscapes, mBm is a much better candidate. We briefly present below the 1D mBm, then move to its 2D isotropic and non-isotropic extensions.

A. 1D mBm

The name "multifractional Brownian motion" was introduced in [21] to designate the following generalization of fBm: The mBm with functional parameter $H(t)$ is the zero-mean Gaussian process defined as

$$W_{H(t)}(t) \propto \int_{-\infty}^{0}\left[(t-s)^{H(t)-1/2}-(-s)^{H(t)-1/2}\right]dB(s) + \int_0^t (t-s)^{H(t)-1/2}dB(s), \qquad (5)$$

where H is a C^1 function ranging in $(0,1)$. A harmonizable representation of mBm was introduced independently in [22]. The increments of mBm are in general neither independent nor stationary. When $H(t)=H\ \ \forall t$, mBm is an fBm of exponent H. The covariance of mBm reads [23]:

$$R_{W_H}(t,s) \propto |t|^{H(t)+H(s)}+|s|^{H(t)+H(s)}-|t-s|^{H(t)+H(s)}.$$

One can show that, contrarily to fBm, the increments of mBm display LRD for all admissible functions $H(t)$ (of course, the notion of long range dependence must be redefined carefully for non-stationary increments, see [23]).

The main feature of mBm is that its Hölder exponent varies in time: At each point t_0, it equals $H(t_0)$ with probability one. This is in sharp contrast with fBm, where the almost sure Hölder exponent is constant: As announced above, mBm allows to describe phenomena whose regularity evolves in time/space. Equally with probability one, the Hausdorff and box dimensions $[c,d]$ are both equal to $2-\min\{H(t), t\in[c,d]\}$. Another important property of mBm is that it is *asymptotically locally self-similar*. Basically, this means that, at each t, there exists an fBm with exponent $H(t)$ which is "tangent" to the mBm: A path of an mBm is thus a "lumping" of infinitesimal portions of fBm-s with well-chosen exponents [22].

Let us finally mention that one can define a generalized mBm where the function H is no longer restricted to be C^1 but may be very irregular. This allows to model Gaussian processes with arbitrary local regularity, and is a useful tool for applications such as image segmentation [24].

B. Two-dimensional extensions of mBm

One can imagine various extensions of mBm in higher dimensions. We describe two versions that are direct generalizations of the ones considered in Section II-A for fBm.

An isotropic *multifractional Brownian field* $W_{H(\mathbf{x})}$ is a centered Gaussian process, whose covariance function de-

pends on a deterministic function $H(\mathbf{x}), \mathbf{x} \in \mathbb{R}^2$ and reads:

$$E\left\{W_{H(\mathbf{x})}(\mathbf{x})W_{H(\mathbf{y})}(\mathbf{y})\right\} \propto \left\{\|\mathbf{x}\|^{H(\mathbf{x})+H(\mathbf{y})} + \|\mathbf{y}\|^{H(\mathbf{x})+H(\mathbf{y})} - \|\mathbf{x}-\mathbf{y}\|^{H(\mathbf{x})+H(\mathbf{y})}\right\}$$

It admits a moving average representation extending in the obvious way (5) to several dimensions.

An anisotropic version called *multifractional Brownian sheet* (mBs) is obtained by extending the definition of the Brownian sheet. For $H : \mathbb{R}^N \to (0,1)^N$ a smooth enough function, the mBs is the centered Gaussian field $F_{H(\mathbf{x})}$ with autocorrelation function:

$$E\left\{F_{H(\mathbf{x})}(\mathbf{x})F_{H(\mathbf{y})}(\mathbf{y})\right\} \propto \prod_{i=1}^{N}\left\{|x_i|^{H_i(\mathbf{x})+H_i(\mathbf{y})}+|y_i|^{H_i(\mathbf{x})+H_i(\mathbf{y})}-|x_i-y_i|^{H_i(\mathbf{x})+H_i(\mathbf{y})}\right\}$$

with $\mathbf{x} = (x_i)_{1\le i\le N}$ and $\mathbf{y} = (y_i)_{1\le i\le N}$ ($N = 2$ for images). As in 1D, one can study the regularity properties of these two fields, and show that their Hölder exponents are controlled by the function H. Multifractional Brownian fields have been used in [25] for the modeling of X-ray images of bones in view of early detection of osteoporosis. Another application is fine terrain modeling ([26]).

V. How to Analyze and Synthesize Fractal Surfaces

A. Analysis

One of the most popular method for estimating the Hurst parameter of a fractal field is based on the wavelet analysis (WA). Being scaled and translated versions of a single oscillating function, wavelets [27] perform a mathematical zooming into signals. In the two-dimensional case, wavelets (and wavelet packets) also provide an appropriate tool for characterizing fields with fractal features. The most usual way to extend WA to 2 (or higher) dimensions is to consider separable wavelet bases. The underlying notion of scale invariance in the WA naturally relates it to nonstationary self-similar processes, whose statistical properties are invariant under scale changes. This special relation was first pointed out for the 1D fBm [28]: wavelet coefficients of fBm form stationary sequences at a given scale and satisfy a "power-law" property. Applied to the 2D isotropic fBm, this means that the variance of its wavelet coefficients at resolution level j is proportional to $2^{j(2H+2)}$ [29]. Written in logarithmic scale, this leads to a simple method for estimating the Hurst parameter of an isotropic fBm. In the case of 2D separable wavelets, we have three different regression lines allowing to estimate H, corresponding to the horizontal, vertical and diagonal details. A more precise estimation of H can be obtained by making a joint linear regression on all the subbands.

Under some assumptions on the number of vanishing moments of the WA, the same property of stationarization was shown to be consistent with the properties of more general 1D random processes with stationary increments [30], [31], [32] and the results have also been extended to fields with stationary increments of arbitrary fractional order [18].

Other classical methods for estimating the Hurst parameter include the box-counting and the variation method [33], [34], maximum likelihood estimates [35], [36], [37], least squares regression in the spectral domain [38], methods based on the log-periodogram [39], or estimators based on the moments of the increments [40], [41]. The fractal dimension has also been measured by morphological covers [42] or by algorithms adapted to a specific application, but derived from existing methods (e.g., the "reticular cell counting" method [43], related to spectral algorithms or the "fractal interpolation function models" [44]).

B. Synthesis

Several methods have been proposed for synthesizing fractional Brownian fields. Synthesizing fBm's is by no means an easy process, especially if one needs to build large images. The problem lies mainly in the non-Markovian nature of fBm. The Choleski method allows exact synthesis, but a plain implementation requires a large computational time and a large amount of memory. Under some minor restrictions, it is possible to use fast and efficient algorithms for Choleski decomposition, but various approximate methods have also been designed that allow reasonable computer time/memory requirements.

We first describe the steps involved in the Choleski method. We wish to generate samples of an index-H fBm B_H at N equidistant points of $[0,1]$. The discrete increments $\Delta B_H(k/N) = B_H(k/N) - B_H((k-1)/N)$ form a stationary Gaussian sequence with zero mean, and the statistical properties of the vector $\Delta B_H = (\Delta B_H(1/N), \Delta B_H(2/N), \ldots, \Delta B_H(1))$ are determined by its autocovariance matrix A_N. Since A_N is positive definite, it may be written using its Choleski decomposition as $A_N = L_N L_N^T$ where L_N is an invertible lower triangular matrix. Let ΔY_N be an N-sample realization of a unit variance centered white Gaussian noise. Then it is clear that the autocovariance matrix of the random vector $L_N \Delta Y_N$ is exactly A_N. Setting $\Delta B_H = L_N \Delta Y_N$, we thus generate a realization of B_H as $B_H(k/N) = \sum_{p=1}^{k} \Delta B_H(p/N)$. The synthesis of an fBm is now reduced to the computation of L_N from A_N. Note that the procedure above may be applied for synthesizing any discrete Gaussian process. A direct method for general Choleski factorization has complexity $O(N^3)$ and cannot be used for building large traces. Fortunately, when the process is stationary (this is why we work with ΔB_H rather than B_H) and when the samples are equi-spaced, the considered matrix is Toeplitz and one can use fast algorithms, such as the Schur or Levinson ones, which have complexity $O(N^2)$ and need $O(N)$ memory. It is possible to do even better if one forces N to be a power of 2. Such a requirement is common to many methods (e.g. FFT or dyadic wavelet-based algorithms). Then, the *doubling Schur algorithm* ([45]) allows the complexity to be reduced to $O(N(\log_2(N))^2)$. This method was used in [46] to synthesize 1D fBm's with 131072 sample points and 2D fBm's with 2048×2048 sample points.

Let us now briefly comment on some approximate methods. The oldest one is the midpoint displacement algorithm. In the case of *Brownian* motion, this is the original construction by P. Lévy of the Wiener process. This method has a linear complexity [47]. When $H \neq 1/2$, however, the resulting process has second order properties that differ significantly from those of fBm. In [48], [37], an improvement of this scheme is proposed, which allows to recover approximately the right covariance function with a low computational burden. The algorithm is based on the notion of a multiscale process, and improves on the classical method by using statistical descriptions of the interpolation and displacement steps.

Wavelet based methods [49] rely mainly on the fact that the wavelet transform acts as a 'whitening filter' on fractional Brownian motion. This allows easy synthesis of the wavelet coefficients of fBm. However, the problem of building the low frequency non-stationary approximation of the signal remains. Other wavelet methods ([50], [29]) assume that the detail coefficients are uncorrelated, thus leading to "$1/f$-type" fields rather than 2D-fBm.

A spectral method for generating an approximation of a two dimensional $N \times N$ fBm is the incremental Fourier synthesis described in [51]. The idea is to create first a periodic random field of size $2N \times 2N$ with statistics close to those of the increments of the 2D-fBm over half the spatial period. Such random fields are easy to generate because their Karhunen-Loève transform is simply the two dimensional discrete Fourier transform. The approximate 2D-fBm is then obtained by adding up the increments. The complexity of this method is $O(N^2 \log_2(N))$. This method can also be used to generate anisotropic fields with stationary increments [52]. Other approximate Fourier methods include the ones described in [3] and [53].

Finally, while methods based on differential models are interesting because they have a physical meaning, they do not yield correct approximations to fBm. In fact, these methods are used to study generic '$1/f$' noises ([54]).

Let us now discuss the synthesis of mBm. The usual technique is based on the property that a path of an mBm with function $H(t)$ is "tangent" at each t_0 to the one of an fBm with exponent $H_0 = H(t_0)$ (see [21]). This allows to generate a sample path of an mBm $B_{H(t)}(t)$ at the N points (t_i) by generating first N plain fBm-s B_i with exponents $H_i = H(t_i)$. One then lumps together the appropriate points $B_i(t_i)$. The complexity of the procedure is $O(N^2(\log_2(N))^2)$. An alternate method is to make use of the Choleski decomposition to generate directly the samples of an mBm. The complexity is now $O(N^3)$: This second method is thus more complex than the first one, but it is exact, whereas the previous one is approximate.

VI. Discrete Fractional Models for a Digitized World

Continuous fields, and in particular fractal fields, have to be sampled in order to be processed. Another approach, which may appear much easier to apply in practice, is to define directly discrete-space models. This idea is also supported by the fact that the increments of continuous-space self-similar fields present long-range dependence (LRD) properties. They can be modeled by 2D extensions of *fractionally integrated auto-regressive moving average* (FARIMA) processes, which have been successfully used in finance, hydrology and other applications. The 2D FARIMA fields can be built in an isotropic or anisotropic manner, the latter being much more flexible in taking into account the characteristics of natural scenes. These models also constitute a discrete alternative to the 2D fractional Gaussian noise. Another argument in favor of discrete-space models is that the parameter estimation methods will be directly derived from the classical approaches existing in the literature for time-series analysis.

A. Long-range dependence and fractal processes

For a stationary second-order random process, $(X(k))_{k\in\mathbb{Z}}$, the LRD is defined by the non summability of its autocorrelation function $\Gamma(k)$. In particular, a condition of LRD is the existence of a parameter $d \in (0, 1/2)$ such that: $\lim_{k\to\infty} k^{1-2d}\Gamma(k) = K_\gamma$, with $K_\gamma \in \mathbb{R}_+^*$ or, equivalently, the power spectrum density is divergent at the origin: $\lim_{\omega\to 0} |\omega|^{2d}\mathcal{S}(\omega) = K_\mathcal{S}$ with $K_\mathcal{S} \in \mathbb{R}_+$. Defining $H = 1/2 + d$, the LRD appears for $H \in (1/2, 1)$. A typical example of an LRD process is the (discrete-time) *fractional Gaussian noise (fGn)* described in Section II-A.

Another example of LRD processes are FARIMA processes, also called fractionally differenced noises, which have been introduced by Hosking [55]. The psd of a FARIMA(0,d,0) process is $\mathcal{S}(\omega) = \sigma^2 |\sin(\omega/2)|^{-2d}$. It can be remarked that, for $\omega \to 0$, it is equivalent to that of the fGn. The constraint $d > 0$ leads to LRD, whereas $d < 1/2$ is necessary for finite variance.

B. Gaussian FARIMA models and related anisotropic fields

A possible bidimensional extension of the fractional Gaussian noise [11] is an isotropic field with 2D psd $\mathcal{S}(\omega_x, \omega_y) \propto \left(\omega_x^2 + \omega_y^2\right)^{-2d}$, $0 < d < 1/2$. The link between d and the Hurst parameter is then: $2d = H$. Its discrete-space equivalent is an isotropic 2D FARIMA. This is a zero-mean Gaussian field with psd:

$$\mathcal{S}(\omega_x, \omega_y) \propto \left(\sin^2\frac{\omega_x}{2} + \sin^2\frac{\omega_y}{2}\right)^{-2d}.$$

When $\omega_x \to 0$ and $\omega_y \to 0$, the psd of the 2D FARIMA process tends towards that of the isotropic fGn.

As already pointed out, it is often useful to dispose of an anisotropic model for LRD fields. It can be built in the same way as the isotropic 2D fractionally differenced Gaussian noise, taking into account jointly the long-range dependence properties, the anisotropy and the directionality in the image. A form for the spectral density answering to these requirements is:

$$\mathcal{S}(\omega_x, \omega_y) = \sigma^2 I(\omega_x, \omega_y)^{2(1-d)} A_{\alpha,\varphi}(\omega_x, \omega_y)^{-2}$$

where $A_{\alpha,\varphi}(\omega_x, \omega_y) = (1 - \alpha\cos\varphi)\sin^2\frac{\omega_x}{2} + (1 + \alpha\cos\varphi)\sin^2\frac{\omega_y}{2} - \frac{1}{2}\alpha\sin\varphi\sin\omega_x\sin\omega_y$. This expression is able, on

the one hand, to model an isotropic part: $I(\omega_x, \omega_y) = \sin^2 \frac{\omega_x}{2} + \sin^2 \frac{\omega_y}{2}$, depending only on the fractional coefficient d and capturing the LRD behaviour, and, on the other hand, an anisotropic part $A_{\alpha,\varphi}(\omega_x, \omega_y)$ depending only on $\alpha \geq 0$ and $\varphi \in [0, 1)$. A polar coordinates change $(\omega_x, \omega_y) = \omega_r(\cos\omega_\theta, \sin\omega_\theta)$ in the previous expression helps in studying the psd in the neighborhood of the origin of the spatial frequency plane. Indeed, for $\omega_r \to 0$, we get $\mathcal{S}(\omega_r \cos\omega_\theta, \omega_r \sin\omega_\theta) \sim \omega_r^{-4d} \left[1 + \alpha - 2\alpha \cos^2\left(\omega_\theta - \frac{\varphi}{2}\right)\right]^{-1}$ For an LRD field, this spectral density diverges at the frequency $(\omega_x, \omega_y) = (0, 0)$, for $d > 0$. Another constraint comes from the fact that, in order to define the correlation function of the field, the integral of its psd has to be finite, and this leads to $d < \frac{1}{2}$. The form of the psd near the origin also suggest the interpretation of the parameters characterizing the model (see Fig. 4). The parameter $\varphi/2 \in [0, \pi)$ determines the orientation of the resulting field: the psd is maximum in the neighborhood of the origin for $\omega_\theta = \varphi/2$ and therefore the privileged direction in the field is $\varphi/2 + \pi/2$. The parameter $\alpha \in [0, 1)$ characterizes the dispersion of the psd of the field around this privileged direction and is called the anisotropy coefficient. In particular, we remark that, for $\alpha = 0$, we find an isotropic model. The fractional parameter d determines the degree of "roughness" of the field. The closer d to 1/2, the "smoother" the field. Note also that the LRD and the anisotropy terms being separated when $\omega_r \to 0$, the orientation and the roughness of the field can be tuned independently. The influence of these parameters on the generated texture are illustrated in Fig. (5).

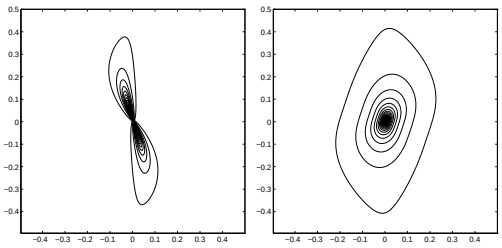

Fig. 4. Level sets of the psd of the anisotropic fractional Gaussian noise, for: $\varphi = -\pi/5, \alpha = 0.97, d = 0.3$ (left) $\varphi = \pi/5, \alpha = 0.17, d = 0.3$ (right). The angle $\varphi/2$ is measured clockwise w.r.t. the vertical axis.

The four parameters of the model: σ^2, d, α, φ, can be easily estimated in the noise-free case, either by a least mean squares approach, or by maximum likelihood [14]. The first method relies on the fact that an asymptotically unbiased estimator of $\log \mathcal{S}(\omega_x, \omega_y)$ is, for $(\omega_x, \omega_y) \neq (0, 0)$, $\log P_N(\omega_x, \omega_y) + \gamma$ ($\gamma \cong 0.57721$), where $P_N(\omega_x, \omega_y)$ is the periodogram of the observed image. In the second case, one can use the Whittle spectral approximation to derive an explicit form for the log-likelihood [56], [57]. When the realizations of the anisotropic FARIMA are corrupted by an additive Gaussian noise, the direct estimation of parameters from the log-likelihood expression leads to a complex non-linear optimization. This can be alleviated by an "expectation-maximization" (EM) approach [58]. At each iteration of the algorithm, an optimization of the same complexity as that of the noiseless model is performed.

C. Non stationary extensions

It is also important to note that it is possible to propose nonstationary extensions of the FARIMA 2D fields [14]. A construction of such fields has been detailed in [59]: starting from a stationary field $(U(n, m))_{(n,m)\in\mathbb{Z}^2}$, we first filter it by the filters with frequency responses

$$G_x(\omega_x, \omega_y) = (1 - e^{-\jmath\omega_x}) \left[\sin^2\left(\frac{\omega_x}{2}\right) + \sin^2\left(\frac{\omega_y}{2}\right)\right]^{-1/2}$$

and $G_y(\omega_x, \omega_y) = G_x(\omega_y, \omega_x)$. The resulting fields B_x and B_y are stationary and can be considered as the increments of a non-stationary field $F(n, m)$ with stationary increments of order (1,0)/(0,1). This one can be constructed by summing up in an appropriate way B_x and B_y. Moreover, if the original field $U(n, m)$ is the anisotropic FARIMA field defined in Section VI-B, then $(F(n, m))_{(n,m)\in\mathbb{Z}^2}$ is a field with stationary increments of order $(\alpha, 0)/(0, \alpha)$, for all $\alpha \in \mathbb{R}$, $\alpha > 2d$. Therefore, these fields are the discrete-space equivalent of the continuous-space models with stationary increments of fractional order discussed in Section III-A. In particular, for isotropic fields, they represent discrete-space counterparts of the isotropic 2D fBm.

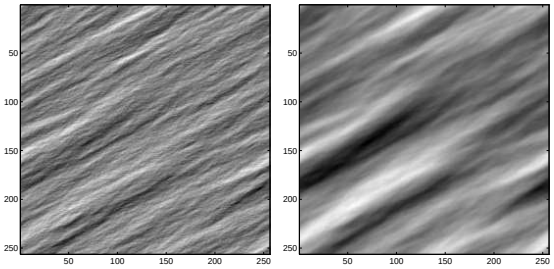

Fig. 5. Left: discrete-space fractional noise with $\varphi = \pi/3, \alpha = 0.97, d = 0.3$. Right: non-stationary field with stationary increments, having the above realization as first-order increment.

D. Non-Gaussian Fractional Fields

The driving noise in the discrete anisotropic model discussed so far has a Gaussian distribution. A large class of distributions can be approximated by Gaussian mixtures and texture models combining such distributions with LRD characteristics have been proposed in [60]. However, in some applications (e.g. SAR, ultrasound or astronomical imaging), the analyzed fields may be highly variable and it may be interesting to use "heavy" tail probability distributions. In particular, stable processes have turned out to be good models for many impulsive signals and noises. Alpha-stable distributions have infinite variance, undefined higher-order moments and, in general, there does not exist an explicit form for their probability densities [61], [10]. They are however interesting in linear modeling, as linear transforms preserve the distribution of any linear combination of i.i.d. α-stable random variables. Alpha-stable 2D discrete-space processes having LRD properties have been studied in [62].

VII. Multifractal Surfaces

Multifractal analysis is concerned with the study of the regularity structure of functions or processes, both from a local and global point of view. More precisely, one starts by measuring in some way the pointwise regularity, usually with some kind of Hölder exponents (see Section II-A or [12]). The second step is to give a global description of this regularity. This can be done in a geometric fashion, using Hausdorff dimension, or in a statistical one through a large deviation analysis. We describe below a simplified version of multifractal analysis in the framework of image processing. Let $X(t)$, $t \in T = [0,1]^2$ denote the image.

The *Hausdorff spectrum* $f_h(\alpha)$ describes the structure of the function $t \mapsto \alpha(t)$ (where $\alpha(t)$ is the Hölder exponent at t) by evaluating the size, as measured by the Hausdorff dimension, of its level sets. In other words, one sets $f_h(\alpha) = \dim_H\{t \in T, \alpha(t) = \alpha\}$, where $\dim_H(E)$ denotes the Hausdorff dimension [63] of the set E. Since each E_α is included in T, f_h takes values in $[0,2] \cup \{-\infty\}$ (the value $-\infty$ occurs when E_α is empty, while $f_h(\alpha_0) = 2$ indicates that a whole region in the image has exponent α_0). ¿From a heuristic point of view, the Hausdorff multifractal spectrum thus describes the "size" of the set of pixels in the image which have a given regularity. For instance, if $f_h(\alpha_0) = 2$ for some $\alpha_0 > 2$ and $f_h(\alpha) < 2$ for all $\alpha \neq \alpha_0$, then we know that almost all points in the image have regularity α_0 and thus that the image is almost everywhere smooth, because $\alpha_0 > 2$.

Another global description of the local regularity is provided by the *large deviation multifractal spectrum*, $f_g(\alpha)$. A heuristic way to introduce f_g is as follows. Fix an integer n and partition the image into n^2 boxes of size $1/n^2$. Now pick a box at random. One defines $f_g(\alpha)$ by writing that the probability that the chosen box has a regularity α behaves as $n^{-(2-f_g(\alpha))}$, when n is large. Thus, roughly speaking, $f_g(\alpha)$ measures the rate of decay, when n tends to infinity, of the probability that a randomly picked region of size $1/n^2$ has regularity α. In particular, if $f_g(\alpha)$ is strictly smaller than 2, then the probability of observing a regularity α goes to 0 exponentially fast, with exponential rate $2 - f_g(\alpha)$: when n is "large", "most" pixels have an α such that $f_g(\alpha) = 2$. We mention that it is natural to interpret f_g as a rate function in a large deviation principle. The theory of Large Deviations provides conditions under which such rate functions may be calculated as Legendre transforms of moment generating functions. When applicable, this procedure yields a more robust estimation than a direct computation. In general, this allows to define a new spectrum, the *Legendre spectrum*, not considered here.

Multifractal analysis has been the subject of numerous studies both in the deterministic and random cases. A very partial list of references is [64], [65], [66], [67], [68]. Many works have been devoted to the comparison of the spectra and their computation in various cases. In particular, it is shown for instance in [69] that the inequality $f_h \leq f_g$ holds in full generality. The spectra have been determined most notably in the case of multiplicative cascades [70], for which one has equality between f_h and f_g (one then says that the multifractal formalism holds). The Hausdorff spectrum of Lévy processes was computed in [71], and the f_h and f_g spectra of a large class of Gaussian processes are given in [72]. Multifractal analysis has a number of important applications in image processing, some of which are described in the next section.

VIII. Applications

Some application of the fractal modeling of surfaces have already been mentioned, like texture analysis and synthesis, others will be discussed in this section.

A. Geophysical fields simulation

A popular way to synthesize various geophysical phenomena is to use multifractals. The starting point of the method is based on the remark that the simplest models leading to processes with non-trivial spectra (*i.e.* not reduced to a point) are the so-called *multiplicative cascades*, and that these kinds of cascades are believed to occur commonly in many natural phenomena. To construct the crudest cascade, choose a real number m_0 in $(0,1)$ and set $m_1 = 1 - m_0$ (these are called the "weights"). Split the unit interval into two halves, and assign measure m_0 to $[0,1/2]$ and measure m_1 to $[1/2,1]$. Iterate this process so that at step n we are dealing with dyadic intervals $[k2^{-n}, (k+1)2^{-n}]$, each having a given measure $\mu_{n,k}$. Then split each of these interval into two halves, and put measure $m_0\mu_{n,k}$ on the left one and measure $m_1\mu_{n,k}$ on the right one. One shows that this procedure allows to define a limiting measure when n tends to infinity, called the *binomial measure*. The binomial measure has a multifractal spectrum looking like the mathematical symbol $\bigcap$. More complex versions of these multiplicative processes are expected to be good models in a wide variety of fields including turbulence [68], [67], DLA [73], financial data modeling [74], Internet traffic [75], [76], geophysics [77], ... In particular, random multiplicative cascades with a continuous scale parameter (*i.e.* defined on a continuum of scales rather than dyadic ones) and a Lévy stable distribution for the weights were used in a series of works [78] to model various multidimensional geophysical phenomena, including clouds and oceans.

Let us finally mention another method for synthesizing clouds based on a wavelet model called TAON [79]. Images obtained with this model are displayed on Fig. 6.

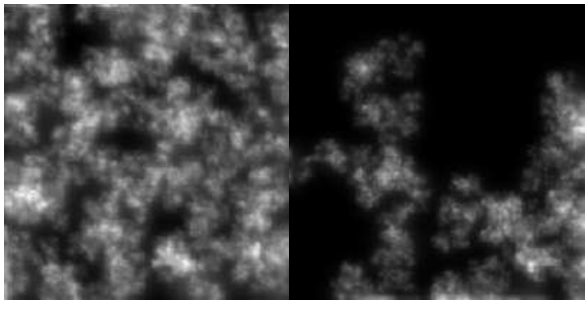

Fig. 6. Cloud images obtained using TAON.

B. Medical applications

Fractal Brownian fields have been early used to model textures and the Hurst parameter has been estimated in view of segmentation and classification [80], [81], [82]. Recently, isotropic and non-isotropic 2D fBm and multifractional Brownian fields have been used for early detection of osteoporosis from X-ray images [25], [83].

C. Satellite imaging

An isotropic FARIMA model with a non-Gaussian (one-sided exponential) white noise driving sequence was used in radar [84] to simulate the texture in synthetic aperture radar (SAR) imagery for ocean surveillance. The isotropy of the model was established based on the symmetry of the periodogram for the RADARSAT clutter. This model, combining a LRD part with an ARMA short-range dependence part, was shown to better fit the experimental clutter power spectral density than both a MA model and a simple fractional differencing field. Other applications in SAR imagery concern radar image data classification [85], [86] and the characterization and segmentation of hydrological basins [87], both based on the fractal dimension.

D. Image segmentation

In many applications, the information contained in the local regularity of images is more important than the actual values of the grey levels. A typical example is edge detection: edges are not modified by an affine transformation of the grey levels, while they always correspond to low regularity pixels. It thus seems reasonable to expect that estimating the Hölder exponents of the image will yield relevant information for segmentation. In the specific case of edge detection, one needs an additional, global, information. Indeed, the property of being an edge point is not only local: by definition, the set of the edges in the image has the geometry of a set of lines (as opposed to 2D regions or isolated points), and thus must be of dimension 1. From a different, statistical, point of view, one also has that the probability that a randomly chosen pixel in an image of size n^2 pixels is an edge point should be of the order of $1/n$. We may then characterize edges as points which have specific, low regularities (this is a local criterion, measured through the Hölder exponent α) and such that the associated spectra value are $f_h(\alpha) = 1$ (because edges are 1D objects) and $f_g(\alpha) = 1$ (because they have a given, resolution-dependent, probability to occur). Multifractal edge detection thus consists in first estimating f_g and then classifying as edge points those pixels whose Hölder exponent α is such that $f_g(\alpha) = 1$ (one assumes that the multifractal formalism is valid, *i.e.* $f_h = f_g$). An example of a multifractal segmentation is displayed on figure 7. See [8] for more on this topic.

E. Image denoising

The problem of image denoising may also be treated with multifractal methods. Intuitively, it seems clear that most points in a scene whose overall appearance is noisy (as for instance SAR images) will have a low regularity. To the contrary, "smooth" images contain mostly points with high values of α. In terms of the multifractal spectrum, noisy images have a "large" $f_g(\alpha)$ for "small" values of α, and have $f_g(\alpha) < 2$ for $\alpha \geq 2$. For "clean" images, $\sup_{\alpha<2} f_g(\alpha) < 2$, and the maximum of f_g is reached for exponents larger than 2. In order to denoise an image, a natural idea is then to modify it so that its multifractal spectrum is translated towards large values of α: in this way, the regularity of each point is increased, but the shape of the spectrum is left unchanged. As a consequence, the image becomes more readable while the respective strength of each singularity remains the same (i.e. a noisy point on a contour will still be, after processing, more irregular than a noisy point in a smooth zone). From a practical point of view, the shift in Hölder regularity is obtained through a non linear manipulation of the wavelet coefficients of the image (see [88] for a detailed explanation). This method allows in particular to process efficiently certain SAR images which resist most other techniques, as shown in Fig. 8.

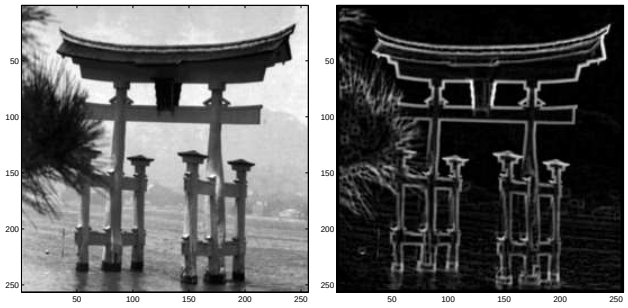

Fig. 7. Original image (left) and edges obtained through multifractal segmentation (right).

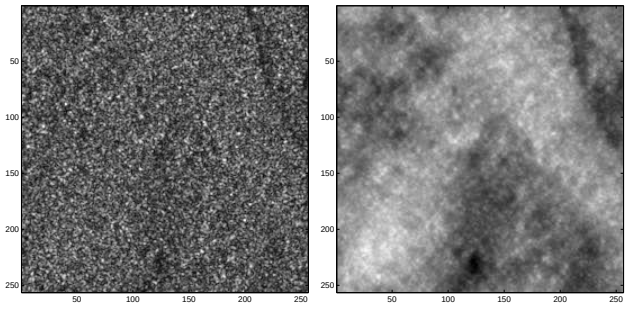

Fig. 8. Original SAR image (left) and its multifractal denoising (right): the multifractal spectrum of the image is shift through a non linear manipulation of its wavelet coefficients.

F. Interpolation of fractal surfaces

In missing data problems, one can be interested in realizing a linear interpolation of a field exhibiting fractal features. The statistical interpolation of nonstationary fields (as those we have seen so far) does not enter the classical framework of mean-square prediction problems for stationary processes [89]. However, if we restrict our analysis to fields having stationary increments, it is possible to extend

the existing methods, by exploiting the properties of the structure function [90]. Indeed, let $F(\mathbf{n})$ be the value of the field to be estimated and $\mathcal{S}$ be a finite subset of $\mathbb{Z}^n \setminus \{\mathbf{0}\}$ which defines a finite neighbourhood $\{\mathbf{n}-\mathbf{p},\, \mathbf{p} \in \mathcal{S}\}$ of the point $\mathbf{n}$. Remark that we do not impose any constraint on the neighbourhood, which can be symmetric or not. The filter is shift-invariant (i.e. its coefficients do not depend on the position $\mathbf{n}$ of the estimated sample) if $\sum_{\mathbf{p}\in\mathcal{S}} h_{\mathbf{n}}(\mathbf{p}) = 1$. The interpolation coefficients are estimated by minimizing the mean square estimation error, and the problem reduces to a linear mean square estimation. As the increments of F are stationary, we can express the normal equations, using the structure function. Together with the shift invariance constraint, we obtain a set of linear equations allowing to determine the impulse response of the interpolation filter. This method has been applied to the interpolation of underwater terrain maps in [90]. Note that the described approach is strongly related to kriging methods [19].

IX. Conclusions

Resulting from more than a century of theoretical works realized in mathematics and physics, the idea of fractals has emerged in the early 1970's. As we have shown in the paper, this concept provides new sophisticated analysis and synthesis tools for image processing. An important question that could be raised at this point is whether fractals constitute adequate models for real scenes. Recent advances [91] have shown that even though few natural images are actually fractal, methods inherited from the fractal and multifractal formalisms can be successfully applied to a wide range of textures and images.

References

[1] M.F. Barnsley, R. L. Devaney, and B. B. Mandelbrot, *The Science of Fractal Images*, Springer Verlag, New York, 1988.

[2] M. Dekking, J. Lévy Véhel, E. Lutton, and C. Tricot, *Fractals : Theory and Applications in Engineering*, Springer Verlag, New York, 1999.

[3] O. Peitgen and D. Saupe, Eds., *The Science of Fractal Images*, Springer-Verlag, New York, 1988.

[4] B. B. Mandelbrot and J. W. Van Ness, "Fractional Brownian motions, fractional noises and applications," *SIAM Rev.*, vol. 10, no. 4, pp. 422–437, 1968.

[5] B. B. Mandelbrot, *The Fractal Geometry of Nature*, W.H. Freeman and Company, New York, 1983.

[6] P. Abry, *Ondelettes et Turbulences - Multirésolutions, algorithmes de décompositions, invariance d'échelle et signaux de pression*, Diderot, Editeurs des Sciences et des Arts, Paris, 1997.

[7] A. Arneodo, F. Argoul, E. Bacry, J. Elezgaray, and J.-F. Muzy, *Ondelettes, multifractales et turbulence – de l'ADN aux croissances cristallines*, Diderot, Arts et Sciences, Paris, 1995.

[8] J. Lévy Véhel, "Introduction to the multifractal analysis of images," in *Fractal image encoding and analysis*. Eds. Y. Fisher, Springer Verlag, 1998.

[9] J. Lévy-Véhel, "Fractal approaches in signal processing," *Fractals*, vol. 3, no. 4, pp. 755–775, 1995.

[10] G. Samorodnitsky and M. S. Taqqu, *Stable Non-Gaussian Random Processes: Stochastic Models with Infinite Variance*, Chapman & Hall, New York, 1994.

[11] I.C. Reed, P. C. Lee, and T. K. Truong, "Spectral representation of fractional Brownian motion in n dimensions and its properties," *IEEE Trans. Inf. Theory*, vol. IT-41, no. 5, pp. 1439–1451, Sept. 1995.

[12] K. Kolwankar and J. Lévy Véhel, "A time domain characterization of the fine local regularity of functions," *J. Fourier Anal. Appl.*, vol. 8, no. 4, pp. 319–334, 2002.

[13] P. Flandrin, "On the spectrum of fractional Brownian motion," *IEEE Trans. Inf. Theory*, vol. IT-35, pp. 197–199, Jan. 1989.

[14] B. Pesquet-Popescu, "Modélisation bidimensionnelle de processus non stationnaires et application à l'étude du fond sous-marin," *Thèse de doctorat, Ecole Normale Supérieure de Cachan*, 1998.

[15] P. Flandrin, *Temps-fréquence*, Hermès, Paris, 1993.

[16] M.S. Taqqu, "A bibliographical guide to self-similar processes and long-range dependence," in *Dependence in Probability and Statistics*, pp. 137–162. Eds. E. Eberlain and M.S. Taqqu, Birkhauser, Boston, MA, 1986.

[17] B. Pesquet-Popescu and P. Larzabal, "2D Self-Similar Processes with Stationary Fractional Increments," in *Fractals in Engineering*, pp. 138–151. Eds. J. Lévy Véhel, E. Lutton, C. Tricot, Springer-Verlag, 1997.

[18] B. Pesquet-Popescu, "Wavelet packet analysis of 2D processes with stationary fractional increments," *IEEE Trans. Inf. Theory*, vol. 45, pp. 1033–1038, 1999.

[19] G. Matheron, "Kriging, or polynomial interpolation procedures," *Canadian Mining and Metallurgical Bulletin*, vol. 60, pp. 1041–1045, 1967.

[20] R. S. Sayles and T. R. Thomas, "The spatial representation of surface roughness by means of the structure function: a practical alternative to correlation," *Wear*, vol. 42, pp. 263–276, 1977.

[21] R. Peltier and J. Lévy Véhel, "Multifractional Brownian motion: Definition and preliminary results," *INRIA Research report No. 2645*, 1995, available at www-rocq.inria.fr/fractales/Publications.

[22] A. Benassi, S. Jaffard, and D. Roux, "Gaussian processes and pseudo-differential elliptic operators," *Rev. Mat. Iberoamericana*, vol. 13, 1989.

[23] A. Ayache, S. Cohen, and J. Lévy Véhel, "The covariance structure of multifractional Brownian motion," in *Proc. Int. Conf. on Acoustics, Speech and Signal Processing*, 2000.

[24] A. Ayache and J. Lévy Véhel, "The generalized multifractional Brownian motion," *Statistical Inference for Stochastic Processes*, vol. 3, pp. 7–18, 2000.

[25] S. Leger, "Analyse stochastique de signaux multi-fractaux et estimations de paramètres," *Thèse de doctorat, Université d'Orléans*, 2000.

[26] E. Herbin, "Terrain modeling using multifractional Brownian motion," Preprint, 2001.

[27] S. Mallat, *A Wavelet Tour of Signal Processing*, Academic Press, Boston, 1997.

[28] P. Flandrin, "Wavelet analysis and synthesis of fractional Brownian motion," *IEEE Trans. Inf. Theory*, vol. IT-38, pp. 910–917, Mar. 1992.

[29] C. Henegan, S. B. Lowen, and M. C. Teich, "Two-dimensional fractional Brownian motion: Wavelet analysis and synthesis," in *IEEE Southwest Symposium on Image Analysis and Interpretation*, New York, 1996.

[30] C. Houdré, *Wavelets, probability and statistics: some bridges*, pp. 361–394, J. Benedetto and M. Frazier, Eds. Boca Raton, FL: CRC Press, 1993.

[31] H. Krim and J.-C. Pesquet, "Multiresolution analysis of a class of nonstationary processes," *IEEE Trans. Inf. Theory*, vol. IT-41, no. 4, pp. 1010–1020, July 1995.

[32] L. M. Kaplan and C.-C. J. Kuo, "Extending self-similarity for fractional Brownian motion," *IEEE Trans. Signal Proc.*, vol. 42, no. 12, pp. 3526–3530, Dec. 1994.

[33] Q. Huang, J. R. Lorch, and R. C. Dubes, "Can the fractal dimension of images be measured ?," *Pattern Recognition*, vol. 27, no. 3, pp. 339–349, 1994.

[34] J. M. Keller, R. Crownover, and R. Y. Chen, "Characteristics of natural scenes related to the fractal dimension," *IEEE Trans. Patt. Anal. Mach. Intell.*, vol. 9, no. 5, pp. 621–627, Sept. 1987.

[35] T. Lundahl, S. M. Kay W. J. Ohley, and R. Siffert, "Fractional Brownian motion : A maximum likelihood estimator and its application to image texture," *IEEE Trans. on Medical Imaging*, vol. 5, no. 3, pp. 152–161, Sept. 1986.

[36] M. Deriche and A. Tewfik, "Signal modeling with filtered discrete fractional noise processes," *IEEE Trans. Signal Proc.*, vol. 41, no. 9, pp. 2839–2849, Sept. 1993.

[37] P.W. Fieguth and A.S. Willsky, "Fractal estimation using models on multiscale trees," *IEEE Trans. Signal Proc.*, vol. 44, pp. 1297–1300, 1996.

[38] J. Geweke and S. Porter-Hudak, "The estimation and applica-

tion of long memory time series models," *Journal of Time Series Anal.*, vol. 4, pp. 221–237, 1983.

[39] P.M. Robinson, "Log-periodogram regression of time series with long range dependence," *Annals of Statistics*, vol. 23, pp. 1043–1072, 1995.

[40] J. Istas and G. Lang, "Quadratic variations and estimation of the local Holder index of a Gaussian process," *Ann. Inst. Henri Poincaré Probabilit et Statistiques*, vol. 33, pp. 407–436, 1987.

[41] R. Peltier and J. Lévy Véhel, "A new method for estimating the parameter of fractional Brownian motion," Technical Report no. 2396, INRIA Rocquencourt, 1994.

[42] P. Maragos and F.K. Sun, "Measuring the fractal dimension of signals: morphological covers and iterative optimization," *IEEE Trans. Signal Proc.*, vol. 41, pp. 108–121, 1993.

[43] J.J. Gagnepain and C. Roques-Carmes, "Fractal approach to two-dimensional and three-dimensional surface roughness," *Wear*, vol. 109, pp. 119–126, 1986.

[44] A.I. Penn and M.H. Loew, "Estimating fractal dimension with fractal interpolation function models," *IEEE Trans. on Medical Imaging*, vol. 16, pp. 930 –937, 1997.

[45] G.S. Ammar and W.B. Gragg, "Superfast solution of real positive definitive Toeplitz systems," *SIAM J. Matrix Anal. Appl.*, vol. 9, pp. 61–76, 1988.

[46] K. Falconer and J. Lévy Véhel, "Horizons of fractional Brownian surfaces," *Proc. of the Royal Math. Soc.*, vol. 456, pp. 2153–2178, 2001.

[47] H.O. Peitgen, H. Jurgens, and D. Saupe, *Chaos and Fractals*, Springer Verlag, New York, 1993.

[48] M.M. Daniel and A.S. Willsky, "Modelling and estimation of fractional brownian motion using multiresolution stocastic processes," in *Fractals in Engineering*, pp. 124–137. Eds. J. Lévy Véhel, E. Lutton and C. Tricot, Springer-Verlag, 1997.

[49] F.W. Elliot and A.J. Majda, "A wavelet Monte Carlo method for turbulent diffusion with many spatial scales," *Journal of Computational Physics*, vol. 113, pp. 82–111, 1994.

[50] G. W. Wornell, "Wavelet-based representations for the $1/f$ family of fractal processes," *Proceedings of the IEEE*, vol. 81, no. 10, pp. 1428–1450, Oct. 1993.

[51] L.M. Kaplan and C.C.J. Kuo, "Texture roughness analysis and synthesis via extended self-similar (ESS) model," *IEEE Trans. Patt. Anal. Mach. Intell.*, vol. 17, no. 11, pp. 1043–1055, Nov. 1995.

[52] B. Pesquet-Popescu and P. Larzabal, "Synthesis of nonstationary fields with stationary increments," in *IEE International Conference on Image Processing and Its Applications*, Dublin, Ireland, 14-17 Juillet, 1997, pp. 303–307.

[53] L.M. Braton and N.R. Bartley, "Simulation of fractal multidimensional images using multidimensional recursive filter," *IEEE Trans. on Circuits and Systems*, vol. 41, pp. 181–188, 1994.

[54] M. S. Keshner, "1/f noise," *Proceedings of the IEEE*, vol. 70, no. 3, pp. 212–218, March 1982.

[55] J. R. M. Hosking, "Fractional differencing," *Biometrika*, vol. 68, no. 1, pp. 165–176, 1981.

[56] P.J. Brockwell and R. A. Davis, *Time Series: Theory and Methods*, Springer-Verlag, New York, 1995.

[57] J. Beran and N. Terrin, "Estimation of the long-memory parameter, based on a multivariate central limit theorem," *Journal of Time Series Analysis*, vol. 15, no. 3, pp. 269–278, 1994.

[58] B. Pesquet-Popescu and P. Larzabal, "Analyse de textures à l'aide de modèles anisotropes à longue dépendance," in *Colloque GRETSI'97*, Grenoble, France, 15-19 Sept., 1997, pp. 635–638.

[59] B. Pesquet-Popescu, "Modèles fractionnaires bidimensionnels à espace discret," *Technique et science informatiques*, vol. 20, pp. 1173–1200, 2001.

[60] B. Pesquet-Popescu and J.-C. Pesquet, "Non-Gaussian anisotropic 2D models with long-range dependence," in *Proc. IEEE Workshop on Non-linear Signal and Im. Proc.*, 1999.

[61] M. Shao and C. L. Nikias, "Signal processing with fractional lower order moments: Stable processes and their applications," *Proc. IEEE*, vol. 8, no. 7, pp. 984–1009, July 1993.

[62] B. Pesquet-Popescu and J.-C. Pesquet, "Bidimensional α-stable models with long-range dependence," in *Proc. IEEE Workshop on Non-linear Signal and Image Proc.*, 1999.

[63] K. Falconer, *Fractal geometry*, John Wiley & Sons Ltd., Chichester, 1990, Mathematical foundations and applications.

[64] M. Arbeiter and N. Patzschke, "Random self-similar multifractals," *Math. Nachr.*, vol. 181, pp. 5–42, 1996.

[65] G. Brown, G. Michon, and J. Peyrière, "On the multifractal analysis of measures," *J. Statist. Phys.*, vol. 66, no. 3-4, pp. 775–790, 1992.

[66] S. Jaffard, "Multifractal formalism for functions II: self-similar functions," *SIAM J. Math. Anal*, 1993.

[67] U. Frisch and G. Parisi, "On the singularity structure of fully developed turbulence," in *Turbulence and predictability in geophysical fluid dynamics and climate dynamics*, M. Ghil, R. Benzi, and G. Parisi, Eds., pp. 84–88. North-Holland, New York, 1985.

[68] B.B. Mandelbrot, "Intermittent turbulence in self similar cascades : divergence of high moments and dimension of the carrier," *J. Fluid. Mech.*, vol. 62, no. 331, 1974.

[69] J. Lévy Véhel and R. Vojak, "Multifractal analysis of Choquet capacities," *Adv. in Appl. Math.*, vol. 20, no. 1, pp. 1–43, 1998.

[70] J. Barral, "Continuity of the multifractal spectrum of a statistically self-similar measure," *J. Theo. Prob.*, vol. 13, no. 4, pp. 1027–1060, 2000.

[71] S. Jaffard, "The multifractal nature of Lévy processes," *Prob Th. Rel. Fields*, vol. 114, no. 2, pp. 207–227, 1999.

[72] C. Houdré and J. Lévy Véhel, "Multifractal spectra of certain stochastic processes," Preprint, 2001.

[73] H.G.E. Hentschel, "Stochastic multifractality and universal scaling distributions," *Phys. Rev. E*, vol. 50, pp. 243, (1994.

[74] L. Calvet and A. Fisher, "Forecasting multifractal volatility," .

[75] J. Lévy Véhel and B. Sikdar, "A multiplicative multifractal model for TCP traffic," in *ISCC*, 2001.

[76] P. Mannersalo and I. Norros, "Multifractal analysis of real atm traffic: a first look," 1997.

[77] F. Schmitt, D. Schertzer, S. Lovejoy, and Y. Brunet, "Empirical study of multifractal phase transitions in atmospheric turbulence," *Nonlin. Proc. in Geophysics*, vol. 1, no. 2, pp. 95–104, 1994.

[78] S. Lovejoy, D. Schertzer, Y. Tessier, and H. Gaonac'h, "Multifractals and resolution-independent remote sensing algorithms: the example of ocean colour," *Int. J. Remote Sensing*, vol. 22, no. 7, pp. 1191–1234, 2001.

[79] A. Benassi, S. Cohen, S. Deguy, and Istas J., "Self-similarity and intermittency," to be published in: Wavelets and Signal Processing, L. Debnath ed., Birkhauser; available at http://llaic3.u-clermont1.fr/∼deguy/publi/index.html.

[80] L.M. Kaplan, "Extended fractal analysis for texture classification and segmentation," *IEEE Trans. Image Proc.*, vol. 8, pp. 1572 –1585, 1999.

[81] H. Potlapalli and R.C. Luo, "Fractal-based classification of natural textures," *IEEE Trans. on Industrial Electronics*, vol. 45, pp. 142 –150, 1998.

[82] Szu-Chu L. and Shyang C., "Dimension estimation of discrete-time fractional brownian motion with applications to image texture classification," *IEEE Trans. Image Proc.*, vol. 6, pp. 1176 –1184, 1997.

[83] R. Jennane, W.J. Ohley, S. Majumdar, and G. Lemineur, "Fractal analysis of bone x-ray tomographic microscopy projections," *IEEE Trans. on Medical Imaging*, vol. 20, pp. 443 –449, 2001.

[84] J. Ilow and H. Leung, "Self-similar texture modelling using FARIMA processes with application to satellite images," *IEEE Trans. Image Proc.*, vol. 10, pp. 792–797, 2001.

[85] C. Jung-Jae and L. Chyi-Chyng, "Sea clutter rejection in radar image using wavelets and fractals," in *Proc. ICIP*, 1997, vol. 2, pp. 354 –357.

[86] E.D. Jansing, D.L. Chenoweth, and J. Knecht, "Feature detection in synthetic aperture radar images using fractal error," in *Proc. IEEE Aerospace Conference*, 1997, vol. 1, pp. 187 –195.

[87] H. Maitre and M. Pinciroli, "Fractal characterization of a hydrological basin using SAR satellite images," *IEEE Trans. on Geoscience and Remote Sensing*, vol. 37, pp. 175–181, 1999.

[88] J. Lévy Véhel, "Signal enhancement based on Hölder regularity analysis," *IMA Volumes in Mathematics and its Applications*, to appear; available at www-rocq.inria.fr/fractales/Publications.

[89] S. Kay, "Some results in linear interpolation theory," *IEEE Trans. on Acoustic, Speech and Signal Proc.*, vol. 31, no. 3, pp. 746–749, June 1983.

[90] B. Pesquet-Popescu and P. Larzabal, "Interpolation of nonstationary fields with stationary increments," in *Proc. ICASSP*, Seattle, USA, 1998, vol. IV, pp. 2197–2200.

[91] Y. Fisher, *Fractal Image Encoding and Analysis*, Springer Verlag, 1998.